

Robust estimation of PCSA and geometric reconstruction for human skeletal muscle

Dongwoon Lee^a, Kajeandra Ravichandiran^b, Ken Jackson^a, Eugene Fiume^a, Anne Agur^b

^a*Department of Computer Science, University of Toronto, Ontario, Canada*

^b*Department of Surgery, University of Toronto, Ontario, Canada*

Abstract

Understanding muscle architecture is crucial to determining the mechanical function of muscle during body movements, because architectural parameters directly correspond to muscle performance. Accurate parameters are thus essential for reliable simulation. Human cadaveric muscle specimen data provides the anatomical detail needed for in-depth understanding of muscle and accurate parameter estimation. However, as muscle generally has non-uniform architecture, parameter estimation, specifically, physiological cross-sectional area (PCSA), is rarely straightforward. To deal effectively with this non-uniformity, we propose a geometric approach in which a polygon is sought to best approximate the cross-sectional area of each fascicle by accounting for its three-dimensional trajectory and arrangement in the muscle. Those polygons are then aggregated to determine PCSA and volume of muscle. Experiments are run using both synthetic data and muscle specimen data. From comparison of PCSA using synthetic data, we conclude that the proposed method enhances the robustness of PCSA estimation against variation in muscle architecture. Furthermore, we suggest reconstruction methods to extract 3D muscle geometry directly from fascicle data and estimated parameters using the level set method.

Keywords: Skeletal muscle; Muscle Architecture; Computational Geometry; Digitization

1. Introduction

Skeletal muscle has been actively studied in biomechanics to discover its mechanical functions associated with body movement. As muscle functions are closely related to architectural parameters [26], such as pennation angle, fiber length and physiological cross-sectional area (PCSA), musculoskeletal simulation needs their accurate determination. Current biomechanical modeling techniques rely on PCSA to estimate peak muscle force production during body movement [19, 3]. Force predictions are known to be highly sensitive to changes in PCSA [7]. Hence, accurate PCSA determination is important for reliable modeling and simulation. In contrast to pennation angle and fiber length, which can be directly measured, PCSA is generally not straightforward to calculate because the functional capacity of all fibers inside the muscle must be accounted for. Ideally, a cross-sectional plane can be specified with respect to the anatomical axis to identify a complete set of cross-sections of all fibers. In parallel muscle, PCSA is usually well determined in the anatomical plane transverse to the longitudinal

axis of the muscle. For other muscles having more complex architecture, such as pennate and convergent muscles, an appropriate plane in which to determine PCSA may not be so easily defined [20]. Therefore, for robust estimation of PCSA, the underlying muscle architectural variations must be carefully taken into account.

In most muscle models, PCSA is calculated simply as [2, 23]

$$\text{PCSA}[\text{cm}^2] = \frac{\text{mass}[\text{g}] \cdot \cos(\text{pennation angle})}{\text{density}[\text{g}/\text{cm}^3] \cdot \text{fiber length}[\text{cm}]} \quad (1)$$

However, except for parallel muscle having uniform architecture, (1) may lead to inconsistent PCSA estimation, because non-uniformities, such as variable fiber length and pennation angle, occur in the architecture of many other muscles. Furthermore, this algebraic method requires the determination of other parameters, some of which are difficult to estimate accurately. For instance, the commonly used density value of $1.0597\text{g}/\text{cm}^3$ [17], which was derived from unfixed

rabbit and canine muscle tissue, may be inaccurate for human skeletal muscles and generally density varies by hydration and fixation time [25]. Muscle volume can be measured directly by water displacement [14], volume reconstruction from MRI scans [11] or indirectly by dividing muscle mass by density [18]. However, water displacement may include internal tendons in volume calculation and MRI has difficulty in identifying specific muscles and capturing narrow areas. In general, architectural parameters are measured by fascicles selectively sampled from the superficial layer of muscle [16, 24]. For an in-depth understanding of architectural parameters and more reliable quantification, Agur et al. [1], Kim et al. [12] and Rosatelli et al. [22] used dissection to collect and digitize fascicles throughout the entire muscle of a human cadaveric specimen. In contrast to these invasive approaches, David et al. [15] proposed a non-invasive method to reliably reconstruct muscle fiber architecture from dense but noisy diffusion tensor images. Based on the digitized fascicle data, Ravichandiran et al. [20, 21] proposed the Fiber Bundle Element (FBE) method to calculate volume and PCSA by representing muscle geometry by a collection of cylinders. Each fascicle is approximated piecewise by a cylinder, the diameter of which is estimated by the distance to the nearest neighboring fascicle. With complete access to volumetric muscle data and geometrical adaptation to its architecture, their method enjoys more reliable estimation of architectural parameters than do other algebraic methods. However, as the diameter of the circular cylinder which they use is always chosen as the distance to the nearest digitized point on a neighboring fascicle, their method may often underestimate the volume of fascicles that are unevenly spaced within muscle. Also, their pointwise calculation for the distance may lead to an inconsistency under certain circumstances. For example, if a fiber point has no collateral neighbors, the estimated thickness of the associated fascicles may be undesirably enlarged because the cross-section is not parallel to the transverse plane.

Lumped-parameter models are commonly used in a variety of computational musculoskeletal systems. While they are versatile for many applications, they may not simulate reliably *in vivo* muscles having complex architecture due to their oversimplification of muscle structures, such as assuming uniform fiber length and arrangement. By comparing with experimental measurements, previous studies [10, 6] demonstrated that force prediction derived from lumped-parameter models unfaithfully varies with respect to change in

joint angle, especially for complex muscles. Blemker and Delp [4, 5] circumvent this problem by incorporating fiber arrangement with simulated fiber excursions during body movement. For this, they reconstructed muscle surface from MRI and then created hexahedral meshes from the surface using a finite element mesh generator. This allows them to study complex muscle as well as its *in vivo* behavior.

For robust estimation of PCSA, we extend the approaches outlined above. We estimate PCSA using polygons that are approximated by considering all immediate neighboring fascicles. Also, we force cross-sections to be perpendicular to the associated fascicle's orientation. This considerably reduces gaps that may be produced by the FBE method. Our proposed method allows for robust estimation of PCSA, enhancing the accuracy of associated simulations. Furthermore, we suggest a method to reconstruct 3D muscle geometry directly from fascicle data.

2. Methods

2.1. Data acquisition for muscle specimens

Our study is based on data obtained from 24 muscle specimens: 7 specimens for *Extensor carpi radialis bevis (ECRB)*, 7 specimens for *Extensor carpi radialis longus (ECRL)*, 4 specimens for *Pectoralis major (PM)* and 6 specimens for *Supraspinatus (SS)*. Muscle specimens with visible abnormalities, such as muscle atrophy, fat infiltration or surgery, are excluded from the data acquisition. During dissection and digitization, associated skeletons and joints are stabilized in the anatomical position with metal plates and screws. Fascicles are sequentially dissected and digitized from superficial to deep throughout the muscle volume. A MicroScribe G2 digitizer with 0.23 mm accuracy is used to mark trajectories of fascicles with sampled points. The fascicles that are digitized in the same plane from medial to lateral constitute a layer. Digitized fascicles are removed, exposing the next layer about 1–2 mm deeper. To identify fascicles accurately, a surgical microscope is used throughout dissection and digitization. Ethics approval was obtained from the Research Ethics Board at the University of Toronto (Protocol Reference Number: 17108).

2.2. Data generation for synthetic muscle

To test and evaluate our method and compare it to the FBE and algebraic methods, we use both synthetic data

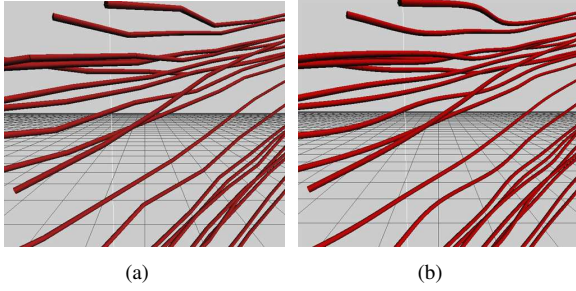


Figure 1: Representation of fascicles. (a) piecewise linear approximation. (b) Catmull-Rom spline interpolation.

and real specimen data. To produce the synthetic data, parametric equations are first chosen to represent targeted geometries: cylinder and ellipsoid. Fascicles are then populated and arranged with respect to predefined architectures: parallel for cylinder (Figure 7) and unipennate for ellipsoid (Figure 8). For each architecture, nonuniform data are also created by varying the interval between fascicles, their length or their pennation angles.

2.3. Reparameterisation of digitized fascicles

Fascicle data is modeled as piecewise lines which simply connect those points (Figure 1(a)). However, this modeling may lead to a poor approximation because fascicles are geometrically closer to smooth curves. Thus, a higher-order representation (Figure 1(b)) is preferable over the piecewise linear approximation. Ravichandiran et al. [20, 21] used the cubic Bézier spline to model fascicles as smooth curves. However, their curves are not guaranteed to pass through all the original points, resulting in geometric deviation from the original data. Instead, we employ a cubic Catmull-Rom spline which ensures that the interpolating curves do pass through all the original points. Like the cubic Bézier spline, a cubic Catmull-Rom spline is a subset of the class of Hermite cubic splines whose tangents are defined by extra control points and a 0.5 tension parameter [8]. Each line segment in the original fascicle is replaced by a cubic and these cubics are joined to form a smooth curve. Once the entire curve is constructed, fiber points are redistributed or resampled to make the curve representation uniform because the original spacing between adjacent points is often irregular. To this end, we use an arc-length parameterisation. An arc-length function $l(t)$ is defined by

$$l(t) = \int_{t_0}^t \left\| \frac{d\mathbf{p}(u)}{du} \right\| du \quad (2)$$

where $\mathbf{p}(u) = (x(u), y(u), z(u))$ represents the curve under consideration. As measured fascicles are generally smooth curves, their arc-length can be approximated by chord-length:

$$l_i \approx \|\mathbf{p}_{i+1} - \mathbf{p}_i\|. \quad (3)$$

Moreover, this approximation is sufficiently good to give a reparameterized spline curve with nearly equal arc-length between points. This is satisfactory for our purpose.

Using (3), a sequence of parameters c_k for $k = 0, \dots, n-1$, can be defined as

$$c_k = \frac{\sum_0^{k-1} \|\mathbf{p}_{i+1} - \mathbf{p}_i\|}{\sum_0^{n-1} \|\mathbf{p}_{i+1} - \mathbf{p}_i\|} \quad (4)$$

c_k denotes the ratio of the chord length from point \mathbf{p}_0 to \mathbf{p}_k over the total length of the entire curve. Using (4), an initial curve representation (c_k, \mathbf{p}_k) is obtained at the original points. We then construct a new set of parameters that is equally spaced by adjusting the interval or sampling rate, producing an interpolated curve (c'_k, \mathbf{p}'_k) (Figure 2). For each specimen, we resample data with 0.5 – 1.0 mm intervals, yielding 50 – 90K points.

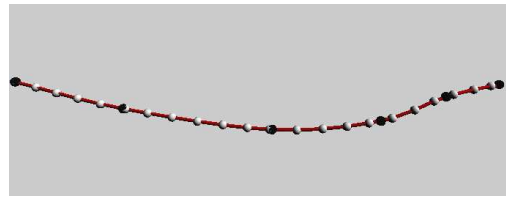


Figure 2: Reparameterisation of fascicle: Original points \mathbf{p}_k (black) and the resampled, evenly spaced points \mathbf{p}'_k (white) on the interpolated curve.

2.4. Estimation of PCSA

Digitized fascicles provide position and orientation information only for muscle. To calculate PCSA, relevant volumetric information must also be recovered. The FBE method [21] is based on the assumption that the volume of connective tissues inside a muscle is negligibly small. Thus, the thickness of a fascicle can be approximated by the distances to neighboring fascicles. Ravichandiran et al. calculate the radius (i.e., half of the thickness) of a fascicle at every fiber point, \mathbf{p} , as

$$r = \min_{\mathbf{q} \in \mathbf{Q}} \|\mathbf{p} - \mathbf{q}\|/2 \quad (5)$$

where \mathbf{Q} is a set of digitized points on neighboring fascicles. Each fascicle is modeled by a piecewise cylinder,

so the average radius, \bar{r} , of the fascicle is given by the mean of the radii of all cylindrical segments, and the resulting PCSA is calculated as

$$\text{PCSA} = \sum_{i=1}^n \pi \bar{r}_i^2 \cos(\alpha_i), \quad (6)$$

where n is the number of fascicles, α_i is the pennation angle of fascicle i . The angle α_i is calculated as the average of the proximal and distal pennation angles of fascicle i . Both angles are measured as the angle between the line of action and tangents at ends of the fascicle (i.e., proximal and distal site) [20, 21]. Because the spacing between fascicles may vary broadly, (5) often underestimates the actual thickness of fascicles in that the smallest circle is always chosen as the best fit (Figure 3). Furthermore, since the radius in (5) is based on pointwise distance within a neighborhood, the distance may not always be perpendicular to the orientation of the fascicle, which could overestimate the thickness of fascicles. This problem may be worse at the ends of fascicles (e.g., tendinous attachments) where fascicles often appear in a staggered pattern. These possible over- and under-estimates compromise the reliability of the PCSA computation, depending on the muscle specimen and digitization accuracy.

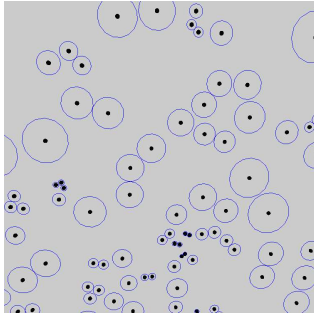


Figure 3: The FBE method. smallest circle (blue) is sought at every fiber point, \mathbf{p} . These points are on the same transverse plane as the one in Figure 4(a).

To improve consistency and reliability, we suggest the following extensions. Instead of the smallest circle, we use a polygon to approximate the cross-sectional area that is formed by a set of points which are equidistant from \mathbf{p} and its neighboring fascicles. Let

$$S(\mathbf{p}) = \{\mathbf{v} | \mathbf{v} = (\mathbf{q} + \mathbf{p})/2, \mathbf{q} \in N(\mathbf{p})\} \quad (7)$$

where $N(\mathbf{p})$ is determined by the intersection of the transverse plane at \mathbf{p} and the neighboring fascicles. In

contrast to the FBE method that chooses among digitized points, \mathbf{q} in (7) can be an arbitrary point on the spline curve representing the fascicle. However, since a cross-section of the fascicle is adjoined by a finite number of neighboring fascicles, only immediate neighbors must be taken into account. Instead of explicitly determining those neighbors, in practice, we use the Voronoi tessellation to directly identify $S(\mathbf{p})$ which consists of vertices and edges equidistant to \mathbf{p} and all its neighbors, \mathbf{q} . Thus, the cross-sectional area, A , at \mathbf{p} , is simply approximated by the polygon formed by $S(\mathbf{p})$ (i.e., Voronoi region) (Figure 4(d)), and the resulting PCSA is calculated as

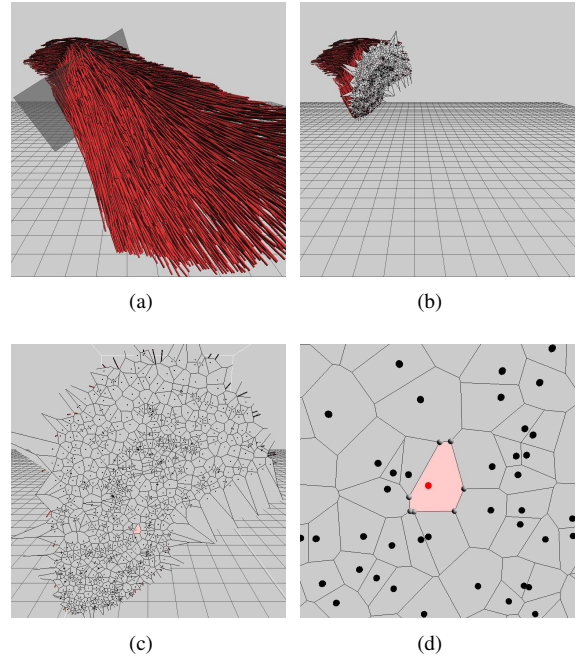


Figure 4: Proposed method. (a) a transverse plane defined at \mathbf{p}_i on the chosen fascicle. (b) Voronoi tessellation. (c)(d) close-up view of Voronoi tessellation with a cross-sectional area A at \mathbf{p}_i (red), approximated as a polygon (pink) defined by $S(\mathbf{p}_i)$ (gray).

$$\text{PCSA} = \sum_{i=1}^n \bar{A}_i \cos(\alpha_i) \quad (8)$$

where \bar{A}_i is the mean cross-sectional area of fascicle i . Figure 4(d) shows that our method always yields a cross-sectional area that is completely filled with polygons, independently of how their centers are arranged, whereas Figure 3 illustrates that this is not the case for the FBE method. Moreover, Figure 3 shows that the FBE method can be quite sensitive to the data, whereas our method is much more robust.

Generally, fascicles located on superficial layers have some degree of deficiency in that they are surrounded by a few neighboring fascicles only, not completely enclosed by them. This may result in an unbounded Voronoi region, the vertices of which are not completely connected. We handle this boundary problem by incorporating an angle-based adjustment:

$$A' = A \frac{2\pi}{\sum_i \text{Angle}(\mathbf{p}, \mathbf{v}_i, \mathbf{v}_{i+1})} \quad (9)$$

where $\text{Angle}(\mathbf{v}_0, \mathbf{v}_1, \mathbf{v}_2)$ is the angle formed by $(\mathbf{v}_0 - \mathbf{v}_1)$ and $(\mathbf{v}_0 - \mathbf{v}_2)$.

2.5. Geometric reconstruction of muscle

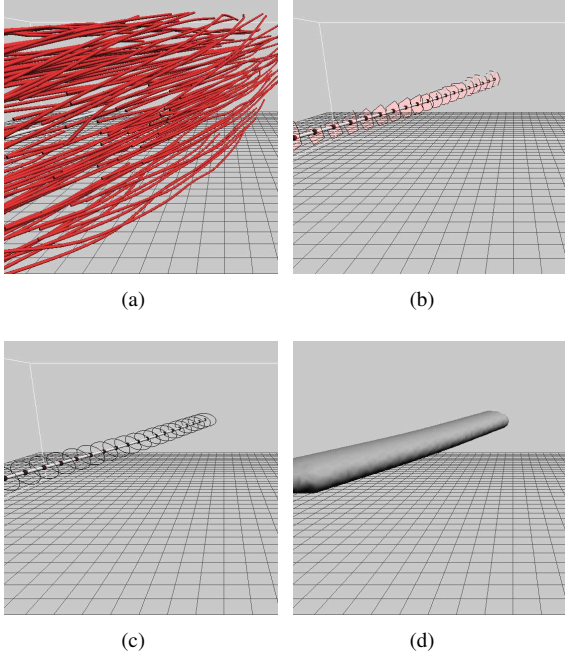


Figure 5: Geometric reconstruction of a single fascicle. (a) a chosen fascicle (white). (b) a series of polygons estimating cross-sections of that fascicle. (c) a series of ellipses to approximate those polygons (d) a reconstructed surface.

To reconstruct muscle geometry from digitized fascicles, their polygonal representation (Figure 5(b)) is further approximated in parametric form, specifically, elliptical cylinders (Figure 5(c)). An ellipse is sought which fits the polygonal cross-section, $S(\mathbf{p})$, by using least-squares-based optimization [9]. Then, a level set method (otherwise known as an implicit surface method) is used to convert the parametric representation into a continuous form (Figure 5(d)). Typically, a

level set function is defined as

$$\phi(\mathbf{x}, \mathbf{p}, r) = \|\mathbf{x} - \mathbf{p}\| - r \quad (10)$$

where \mathbf{x} is a position to be evaluated and r is the desired strength of the field at \mathbf{p} . The set of \mathbf{x} for which (10) is zero forms a bounding solution surface (i.e., isosurface). Taking into account that, in our case, we use ellipses of a particular orientation, we extend (10) to

$$\phi_a(\mathbf{x}', \mathbf{p}, \mathbf{A}) = [(\mathbf{x}' - \mathbf{p})^T \mathbf{A} (\mathbf{x}' - \mathbf{p})]^{\frac{1}{2}} - 1.0 \quad (11)$$

$$\mathbf{A} = \begin{bmatrix} A & B/2 & D/2 \\ B/2 & C & E/2 \\ D/2 & E/2 & F \end{bmatrix}$$

where the symmetric positive-definite matrix \mathbf{A} is built from an ellipse in the quadratic polynomial form, $Ax^2 + Bxy + Cy^2 + Dx + Ey + F = 0$, and \mathbf{x}' is a point which lies on the transverse plane at \mathbf{p} on the fascicle. Equation (11) is evaluated on the transverse plane and swept along the fascicle to create a cylindrical geometry.

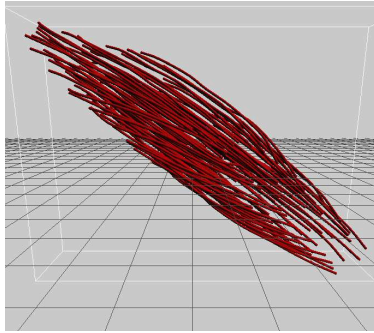
Because fascicles are reconstructed individually, they may become disjoint, thereby separating from each other (Figure 6(b)). To model an entire muscle surface, including all other connective tissues, such as epimysium, perimysium and endomysium, level sets associated with each fascicle should be joined with appropriate overlaps. For this, we use interpolation based on weighted local averaging [27] of neighboring fascicles (Figure 6(c)). To this end, let

$$\phi_p(\mathbf{x}', \bar{\mathbf{p}}, \bar{\mathbf{A}}) = [(\mathbf{x}' - \bar{\mathbf{p}})^T \bar{\mathbf{A}} (\mathbf{x}' - \bar{\mathbf{p}})]^{\frac{1}{2}} - 1.0 \quad (12)$$

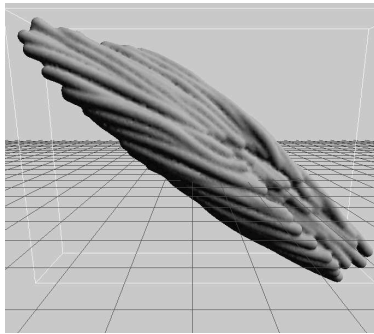
$$\bar{\mathbf{p}} = \sum_i w_i \mathbf{p}_i$$

$$w_i = \frac{k(\|\mathbf{x}' - \mathbf{p}_i\|/R)}{\sum_j k(\|\mathbf{x}' - \mathbf{p}_j\|/R)}$$

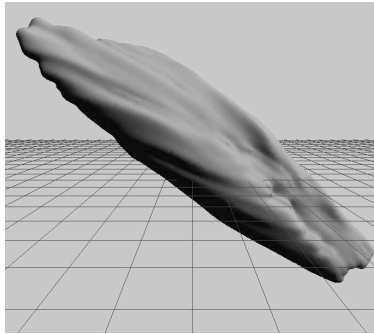
where $\bar{\mathbf{A}}$ represents a locally averaged ellipse and k is a kernel function which is symmetric and smoothly decays with local support, R . We use $k(t) = \text{MAX}(0, (1 - t^2)^3)$. Using (11) or (12), a scalar field is densely sampled on a 3D grid, with spacing specified as 1.0 mm in our study, and the corresponding mesh is extracted using a polygonisation technique. We use a BCC grid-based technique [13] to directly extract a tetrahedral mesh (Figure 6).



(a)



(b)

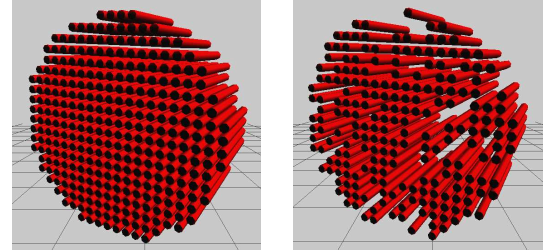


(c)

Figure 6: Reconstruction of muscle geometry. (a) spline-based fascicles. (b) reconstruction of fascicles (without interpolation). (c) reconstruction of entire muscle (with interpolation).

Muscle	Algebraic Method	Our Method	FBE Method
Parallel ¹	78.5	78.7 (+0.3)	61.7(-21.4)
Parallel ²	78.5	79.1 (+0.8)	42.2(-46.2)
Unipennate ¹	97.3	101.8(+4.6)	78.8(-18.9)
Unipennate ²	94.3	102.4(+8.7)	32.6(-65.3)

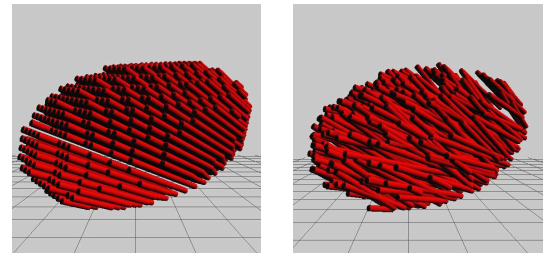
Table 1: Comparative results for PCSA (cm²) using the algebraic method, our proposed method and the FBE method. Superscripts 1 and 2 indicate uniform and nonuniform representation, respectively. Percentage of relative errors are given in parenthesis.



(a)

(b)

Figure 7: Synthetic parallel muscles. Fascicles are created within a cylinder having radius and length of 5 cm and pennation angle of 0. (a) uniform muscle. (b) nonuniform muscle (intervals between fascicles are variable).



(a)

(b)

Figure 8: Synthetic unipennate muscles. Fascicles are created within an ellipsoid, having axes of length 5, 5 and 10 cm. (a) uniform muscle (only fascicle length is variable) (b) nonuniform muscle (fascicle length, pennation angle and interval between fascicles are variable).

Muscle	Volume	Volume ^c	Volume ^f
Parallel ¹	392.7	393.5 (+0.2)	342.3(-12.8)
Parallel ²	392.7	395.5 (+0.7)	350.2(-10.8)
Unipennate ¹	1047.2	979.3(-6.4)	934.1(-10.8)
Unipennate ²	1047.2	981.8(-6.2)	965.9(-7.7)

Table 2: Comparative results for volume (cm³). Volume^c is an approximate volume computed by a collection of cylinders. Volume^f is an approximate volume computed by a tetrahedral mesh. Percentage of relative errors are given in parenthesis.

3. Results

3.1. Synthetic muscle data

As the exact geometry is known for each problem, the algebraic method (1) gives the exact PCSA for the problem. Therefore, we can use this exact value to compute the error associated with either our method or the FBE method. The PCSA results for these three methods and the relative errors for our method and the FBE method are presented in Table 1. The results show that our method performs much more reliably than the FBE method. Note that the FBE method underestimates PCSA by nearly 20% even in uniform muscles. Because spacings between fascicles are equal vertically and horizontally but not diagonally, there are substantial gaps between diagonal neighbors. The larger the variance of those spacings is, the more the gaps between fascicles are not accounted for in FBE method. This results in the FBE method’s vulnerability to nonuniformity of data that often exists in specimen data or can be induced by digitization error. On the other hand, our method considers the entire proximities around fascicles. Hence, it produces more robust PCSA estimates with less sensitivity to data. The results computed by our method are always slightly larger than the results for the algebraic method. This is caused by our treatment of the boundary. As cross-sectional areas of boundary fascicles are adjusted by extrapolation in our method, outer areas located beyond the predefined boundary also are added into our calculation. This adjustment can be larger in nonuniform muscle than in uniform muscle.

Volume estimates are compared in in Table 2. First, the volume (Volume^c) is approximated by a collection of cylinders, formed by cross-sections along the fascicle length. That is, $\sum_{i=1}^n \bar{A}_i l_i$ where \bar{A}_i is the approximate PCSA of fascicle i and l_i is its length. Volume can also be calculated from the reconstructed muscle geometry. Since our approximation to the muscle geometry consists of tetrahedra, muscle volume (Volume^f) is approx-

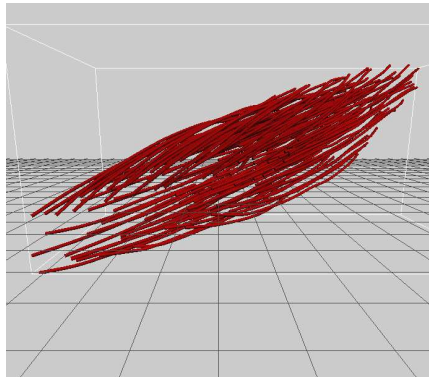
imated by the sum of volumes of tetrahedra. As only fascicle volume is considered, muscle geometry is reconstructed by (11). Volume^c in Table 2 is close to the exact volume. On the other hand, Volume^f in Table2, which is computed from the volume of tetrahedral mesh, has significantly larger errors (8 – 13%). This is caused mainly by errors that arise in both obtaining the parametric form and polygonising the level set surfaces.

3.2. Digitized specimen data

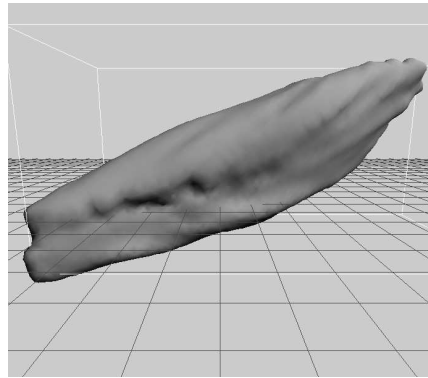
Our PCSA and volume estimation for specimen data are given in Table 3, and a comparison with the FBE method is presented in Table 4. The results clearly show that PCSA and volume vary by specimen and muscle. For geometry reconstruction, a 1 mm grid is used for all specimens except *PM* for which a 2 mm grid is used instead because the size of *PM* demands a tremendous memory allocation. The level-set method performs poorly for *PM* and *SS*, in which many cross-sections of fascicles are estimated to be smaller than the grid-size. Thus, a finer grid must be used to reduce the difference. Similar to the results for synthetic data, our method yields larger PCSA estimation than does the FBE method. The two methods differ by 45 – 50% for *ECRB*, *ECRL* and *PM*, and 20 – 35% for *SS* in specimen to specimen comparison. This may be because *SS* is more uniform than other muscles in terms of fascicle arrangement or cross-sectional area. Note that our FBE results are smaller than the original results [21]. That may be explained by the difference of resampling fascicle data. In our method, fiber points are resampled very densely and equally spaced. That reduces over-estimation for fascicle thickness that point-wise calculation of the FBE method could produce (as discussed in 2.4).

4. Discussion and future work

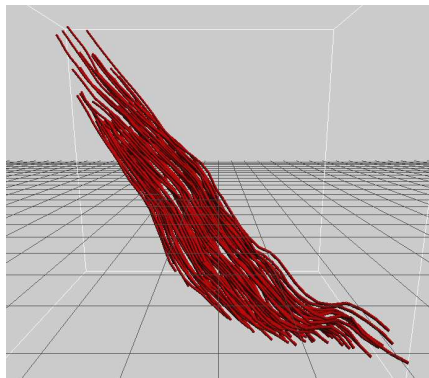
Human cadaveric muscle specimen data provides the potential for an in-depth understanding of human skeletal muscle and accurate parameter estimation. However, most muscles have highly non-uniform architecture, in that their fascicles vary in orientation, thickness and cross-section. Thus, determining the associated parameters, specifically, PCSA, is not straightforward. Furthermore, any measurement error may induce more non-uniformity. Although the algebraic method (1) is commonly used, its accuracy depends on other parameters, such as volume, density, fascicle length and sarcomere length, which are not all easy to approximate well. Even though MRI provides



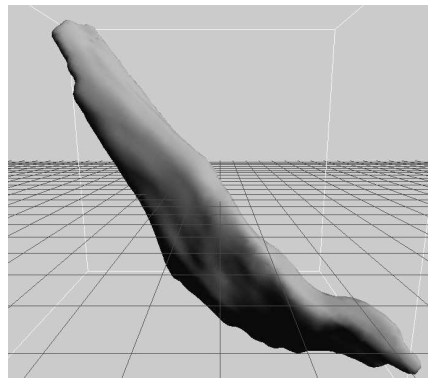
(a)



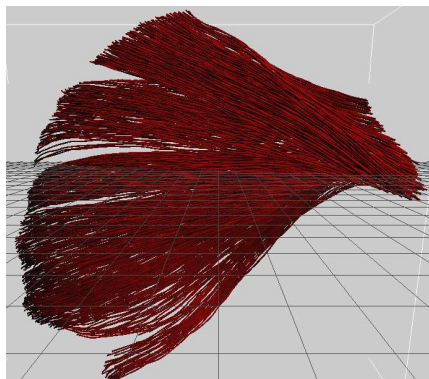
(b)



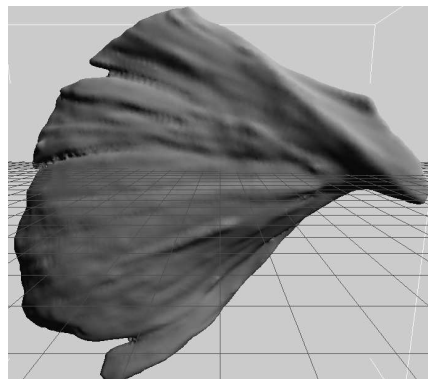
(c)



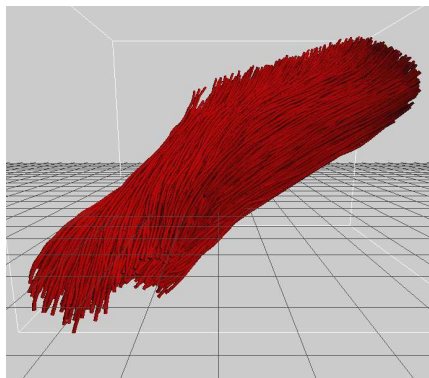
(d)



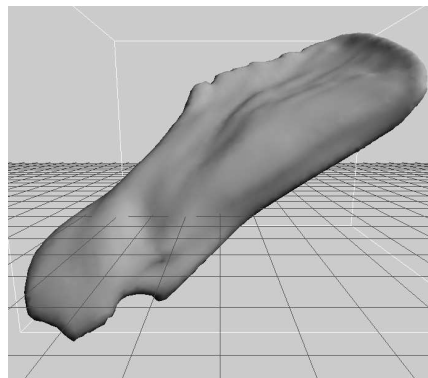
(e)



(f)



(g)



(h)

Figure 9: Reconstruction of muscle geometry. Muscles are illustrated in two representations: fascicles (on left) and reconstructed surface geometry (on right). *ECRB* (a,b), *ECRL* (c,d), *PM* (e,f) and *SS* (g,h).

Muscle	n	PCSA	Volume ^c	Volume ^e
<i>ECRB</i>	128	4.18	21.33	20.33
	93	2.09	12.01	12.23
	117	2.65	17.32	16.36
	106	2.84	18.72	18.24
	106	2.43	14.45	12.18
	178	2.11	8.81	8.47
	126	3.03	16.83	16.22
<i>ECRL</i>	116	4.14	28.37	26.49
	87	1.63	13.37	13.68
	62	1.65	15.66	15.23
	74	2.74	27.92	24.1
	76	1.59	15.54	14.74
	105	1.9	11.86	11.44
	92	2.02	17.67	16.66
<i>PM</i>	634	14.87	277.1	246.78
	679	12.1	224.4	171.36
	767	12.32	206.7	169.69
	873	10.41	188.7	140.3
<i>SS</i>	1750	6.16	45.7	38.23
	1081	5.07	33.7	25.35
	1684	6.31	39.18	28.68
	1061	7.68	38.38	31.71
	1294	7.16	52.26	42.91
	1556	9.16	64.71	53.7

Table 3: PCSA (cm²) and volume (cm³) estimation for specimen data by our method. n is the number of digitized fascicles.

Muscle	Our Method	FBE
<i>ECRB</i>	2.76 ± 0.72	1.26 ± 1.37
<i>ECRL</i>	2.24 ± 0.93	1.13 ± 0.29
<i>PM</i>	12.43 ± 1.84	7.43 ± 0.69
<i>SS</i>	6.92 ± 1.42	4.31 ± 1.49

Table 4: Comparative results for PCSA (cm²) between our method and the FBE method. The number before the ± is the mean PCSA for all specimens of that muscle type in Table 3, while the number after the ± is the associated standard deviation.

direct volume calculation, it has some limitations: difficulty in differentiating specific muscle from others and inaccuracy in narrow areas. The FBE method does not need any other parameters but only uses the coordinates of digitized fascicle data. However, its performance varies with the application. While it works well for uniform data, it shows inconsistency for non-uniform data. We propose an adaptive geometric approach, similar to the FBE method. Our method approximates a collection of fascicles and aggregates their parameters to determine the resulting PCSA. In contrast to the FBE method, our approach endeavors to approximate cross-sectional areas by using a polygon, yielding more robust and consistent estimation of PCSA than previous methods. Furthermore, based on those estimated parameters, we suggest the method to reconstruct the whole muscle geometry by using the level set method. The resulting mesh can be used to visualize the approximated shape of muscle and its dynamic simulation as well. However, its accuracy needs to be assessed by further validation, such as other medical imaging or 3D scanning methodologies.

Although our approach exhibits improved parameter estimation capability compared to earlier approaches, there are some problems to overcome. Firstly, in our PCSA estimation, no connective tissues or other tissues (e.g., blood vessels) are considered. Even though they occupy volume to some extent between fascicles, all partitioned areas are simply included in the PCSA. Thus, our computed PCSA may be slightly larger than the actual PCSA. Secondly, parameterisation of cross-sections needs to be improved. These cross-sections are individually and locally approximated by parametric ellipses. Even though the thickness of a fascicle changes smoothly, our least squares based estimation of serial cross-sections may vary abruptly depending on the availability of their neighbors. Incorporating the correlation between adjacent cross-sections or global constraints may produce more reliable and consistent parameterisation than our localized method does. Thirdly, we use four sets of synthetic data only to validate our method. For a more extensive validation study, we may need to increase the sample size of data (e.g., more random data generated for each architecture) or introduce other variations, such as variable spline curves rather than straight lines. Finally, there is another important aspect of the problem that we currently handle in an ad hoc way. To extract muscle geometry, level sets of all fascicles must be properly interpolated with acceptable overlaps. As the overlap increases, the resulting muscle surface becomes smoother but shrinks. Otherwise,

the surface breaks into disjoint fascicles. Thus, accurate reconstruction of muscle geometry needs the determination of appropriate overlaps, which we leave as a topic for future work.

Acknowledgement

This research was supported in part by the Natural Sciences and Engineering Research Council (NSERC) of Canada.

Conflict of interest statement

We hereby declare that no conflict of interest exists in our study.

References

- [1] Agur, A., Ng-Thow-Hing, V., Ball, K., Fiume, E., McKee, N., 2003. Documentation and three-dimensional modelling of human soleus muscle architecture. *Clinical Anatomy* 16, 285–293.
- [2] Alexander, R., Vernon, A., 1975. The dimensions of knee and ankle muscles and the forces they exert. *Journal of Human Movement Studies* 1, 115–123.
- [3] Anderson, F.C., Pandy, M.G., 2003. Individual muscle contributions to support in normal walking. *Gait & Posture* 17, 159–169.
- [4] Blemker, S., Delp, S., 2005. Three-dimensional representation of complex muscle architectures and geometries. *Annals of Biomedical Engineering* 33, 661–673.
- [5] Blemker, S., Delp, S., 2006. Rectus femoris and vastus intermedius fiber excursions predicted by three-dimensional muscle models. *Journal of Biomechanics* 39, 1383–1391.
- [6] van den Bogerta, A.J., Gerritsena, K.G.M., Cole, G.K., 1998. Human muscle modelling from a user’s perspective. *Journal of Electromyography and Kinesiology* 8, 119–124.
- [7] Branda, R., Pedersen, D.R., Friederich, J.A., 1986. The sensitivity of muscle force predictions to changes in physiologic cross-sectional area. *Journal of Biomechanics* 19, 589–596.
- [8] Catmull, E., Rom, R., 1974. A class of local interpolating splines. *Computer Aided Geometric Design* , 317–326.
- [9] Fitzgibbon, A., Pilu, M., Fisher, R.B., 1999. Direct least square fitting of ellipses. *IEEE Trans. Pattern Anal. Mach. Intell.* 21, 476–480.
- [10] Herzog, W., Keurs, H.E.D.J., 1988. Force-length relation of in-vivo human rectus femoris muscles. *Pflügers Archiv European Journal of Physiology* 411, 642–647.
- [11] Holzbaur, K.R., Murray, W.M., Gold, G.E., Delp, S.L., 2007. Upper limb muscle volumes in adult subjects. *Journal of Biomechanics* 40, 742–749.
- [12] Kim, S., Boynton, E., Ravichandiran, K., Fung, L., Bleakney, R., Agur, A., 2007. Three-dimensional study of the musculotendinous architecture of supraspinatus and its functional correlations. *Clinical Anatomy* 20, 648–655.
- [13] Labelle, F., Shewchuk, J.R., 2007. Isosurface stuffing: fast tetrahedral meshes with good dihedral angles. *ACM Trans. Graph.* 26, 28–37.
- [14] Langenderfer, J., Jerabek, S.A., Thangamanib, V.B., Kuhnc, John E. and Hughes, R.E., 2004. Musculoskeletal parameters of muscles crossing the shoulder and elbow and the effect of sarcomere length sample size on estimation of optimal muscle length. *Clinical Biomechanics* 19, 664–670.
- [15] Levin, D.I., Gilles, B., Madler, B., Pai, D.K., 2011. Extracting skeletal muscle fiber fields from noisy diffusion tensor data. *Medical Image Analysis* 15, 340–353.
- [16] Lieber, R., Friden, J., 2000. Functional and clinical significance of skeletal muscle architecture. *Muscle Nerve* 23, 1647–1666.
- [17] Mendez, J., Keys, A., 1960. Density and composition of mammalian muscle. *Metabolism* 9, 184–188.
- [18] Murray, W.M., Buchanan, T.S., Delp, S.L., 2000. The isometric functional capacity of muscles that cross the elbow. *Journal of Biomechanics* 33, 943–952.
- [19] Pandy, M.G., 2001. Computer modeling and simulation of human movement. *Annual Review of Biomedical Engineering* 3, 245–273.
- [20] Ravichandiran, K., Ravichandiran, M., Oliver, M., Singh, K., McKee, N., Agur, A., 2009. Determining physiological cross-sectional area of extensor carpi radialis longus and brevis as a whole and by regions using 3d computer muscle models created from digitized fiber bundle data. *Comput. Methods Prog. Biomed.* 95, 203–212.
- [21] Ravichandiran, K., Ravichandiran, M., Oliver, M., Singh, K., McKee, N., Agur, A., 2010. Fibre bundle element method of determining physiological cross-sectional area from three-dimensional computer muscle models created from digitized fibre bundle data. *Comput. Methods Prog. Biomed.* 13, 741–748.
- [22] Rosatelli, A., Ravichandiran, K., Agur, A., 2008. Three-dimensional study of the musculotendinous architecture of lumbar multifidus and its functional implications. *Clinical Anatomy* 21, 539–546.
- [23] Sacks, R., Roy, R., 1982. Architecture of the hindlimb muscles of cats: functional significance. *Journal of Morphology* 173, 185–195.
- [24] Ward, S., Kim, C., Eng, C., Gottschalk, L., Tomiya, A., Garfin, S., Lieber, R., 2009. Architectural analysis and intraoperative measurements demonstrate the unique design of the multifidus muscle for lumbar spine stability. *J Bone Joint Surg Am* 91, 176–185.
- [25] Ward, S., Lieber, R., 2005. Density and hydration of fresh and fixed human skeletal muscle. *Journal of Biomechanics* 38, 2317–2320.
- [26] Zajac, F., 1989. Muscle and tendon: properties, models, scaling, and application to biomechanics and motor control. *Critical Reviews in Biomedical Engineering* 17, 359–411.
- [27] Zhu, Y., Bridson, R., 2005. Animating sand as a fluid. *ACM Trans. Graph.* 24, 965–972.